geosciences

MDPI

Article

The Sedimentary Forward Modeling-Based Lithofacies Paleogeographic Distribution of the Ediacaran Dengying Formation, Northeastern Sichuan Basin

Xiang Cheng [1,2], Shengqian Liu [1,2,*], Jinxiong Luo [1], Yan Zhong [1], Dazhi Zhang [3] and Shan Sun [3]

[1] School of Geosciences, Yangtze University, Wuhan 430100, China; 2023710470@yangtzeu.edu.cn (X.C.); luojinxiong1980@126.com (J.L.); zy220623@163.com (Y.Z.)
[2] Hubei Engineering Research Center of Unconventional Petroleum Geology and Engineering, Wuhan 430100, China
[3] Exploration and Development Research Institute of PetroChina Daqing Oilfield Co., Ltd., Daqing 163712, China; dqzhangdzh@petrochina.com (D.Z.)
* Correspondence: liusq@yangtzeu.edu.cn

Abstract

The Sinian (Ediacaran) Dengying Formation in the northeastern Sichuan Basin exhibits a significant exploration potential. Nevertheless, the great burial depth of carbonates in the Dengying Formation and the scarcity of drilling data have imposed constraints on in-depth investigations into the evolution of lithofacies paleogeography as well as the primary controlling mechanisms. Through integrated analysis of field outcrops, core and well logging data, the evolution of the lithofacies and paleogeography of the Dengying Formation in the northeastern Sichuan Basin was reconstructed by using 3D stratigraphic forward modeling. The study area is predominantly characterized by platform margin facies and restricted platform facies, comprising four subfacies including microbial (algal) mound, grain shoal, intershoal sea, and intraplatform depression. The microbial (algal) mound and grain shoal subfacies are primarily developed along the western and eastern platform margins, exhibiting a near north–south trend. Scattered mound–shoal complexes and intershoal sea occur within the platform, with localized intraplatform depression zone. During the depositional stage of the Dengying Formation, three primary paleogeomorphic units were developed including the platform margin topographic high zone, intraplatform gentle slope zone, and intraplatform depression zone. During the Deng-1 and Deng-3 periods, sea level rise increased accommodation space, leading to a gradual decline in carbonate productivity and limited development of the mound–shoal complexes. In contrast, during the Deng-2 and Deng-4 periods, sea level decreased, water depth decreased, and carbonate productivity was enhanced, resulting in extensive development of the mound–shoal complexes. The simulation results indicate that carbonate-producing ecosystems thrive when wind blows from 270° W (80% frequency) or 15° N (60% frequency); with an effective water depth of 10–20 m, the elevated carbonate productivity is conducive to the growth of biogenic calcification. Comprehensive analysis suggests that paleogeomorphology, eustatic fluctuations, and paleowind fields collectively control the distribution and evolution of the lithofacies in the Dengying Formation in the northeastern Sichuan Basin. Paleogeomorphology governs the types and distribution of sedimentary facies belts as well as the spatial arrangement of lithofacies. Eustasy determines the magnitude of mound–shoals and their lateral migration. Three-dimensional stratigraphic forward modeling offers a novel approach for reconstructing paleogeographic evolution of carbonate platforms and analyzing key controlling factors, while also enhancing our ability to predict the distribution patterns of mound–shoal complexes.

Check for updates

Academic Editor: Tadeusz Marek Peryt

Received: 15 December 2025
Revised: 13 February 2026
Accepted: 15 February 2026
Published: 24 February 2026

Copyright: © 2026 by the authors. Licensee MDPI, Basel, Switzerland. This article is an open access article distributed under the terms and conditions of the Creative Commons Attribution (CC BY) license.

Keywords: Sichuan basin; Sinian (Ediacaran); Dengying formation; lithofacies; paleogeography; stratigraphic forward modeling

1. Introduction

The Sichuan Basin is a core basin for marine hydrocarbon exploration in southern China and has long been a crucial hydrocarbon-producing area in the country [1]. In recent years, a series of major exploration breakthroughs have been achieved in the Dengying Formation, providing new insights for hydrocarbon exploration in the Precambrian carbonate reservoirs. The discoveries of the Weiyuan Gas Field, Anyue Gas Field, and Penglai Gas Field have demonstrated the enormous hydrocarbon exploration potential of this formation [2–4]. However, current exploration efforts are mainly concentrated in the platform margin zone of the central Sichuan area, while the exploration degree in the northeastern Sichuan area remains relatively low, with most wells producing at medium to low rates [5]. Regarding the study of the lithofacies paleogeography of the Dengying Formation in the Sichuan Basin, some scholars have proposed that the overall lithofacies paleogeographic pattern of the Dengying Formation is a rimmed platform [6,7]. With the proposal of concepts such as extensional troughs, rifted troughs, and erosional troughs, most scholars now hold the view that the paleogeographic pattern is characterized by the coexistence of uplifts and depressions, with an overall rimmed platform setting [8,9]. This uplift–depression pattern controls the distribution of sedimentary facies belts. In terms of mapping scope, most studies cover the entire basin, while a small number focus on the central Sichuan area and northern Sichuan area [10].

Sedimentary forward modeling serves as a fundamental method for investigating stratigraphic sedimentation [11]. In recent years, it has been widely applied in the analysis of carbonate platform evolution, particularly in regions characterized by deep-buried strata and limited drilling data. By constructing geological models to simulate the sedimentary processes of carbonate platforms across different geological periods, the evolutionary history of platforms can be visualized explicitly—including the migration of platform margins and changes in intraplatform sedimentary environments [12–15]. In studies of modern carbonate platforms, sedimentary forward modeling, when integrated with high-precision topographic survey data and sedimentation rate data, effectively explains the formation mechanism of platform geomorphology and the distribution patterns of different sedimentary facies belts [16,17]. Within the scope of sedimentary evolution research, sedimentary forward modeling is also employed to simulate the evolutionary processes of sedimentary basins under diverse tectonic settings. By defining parameters such as plate movement rate, paleotopographic relief, and sediment supply [18,19], the entire process of a sedimentary basin—from its initial formation to subsequent modification—can be simulated. This facilitates understanding of the basin's formation mechanism, stratigraphic accumulation patterns, and the spatiotemporal distribution of sedimentary facies [20].

Recent years have witnessed the gradual advancement of sedimentary forward modeling studies targeting the Dengying Formation in the Sichuan Basin. In these investigations, most researchers have incorporated key factors—including sea level changes, tectonic activity, and sediment supply—to construct sedimentary forward models, achieving the coupling of tectono-sedimentary filling simulations and hydrocarbon accumulation simulations for the Dengying Formation [21]. These simulations have, to a certain extent, revealed the formation and evolutionary processes of the Dengying Formation's carbonate platforms, providing more intuitive insights into the migration of platform margin and the evolution of intraplatform sedimentary environments across different regions. The Dengy-

ing Formation in the northeastern Sichuan area exhibits distinct regional characteristics: its sedimentary environment was likely more significantly influenced by tectonic factors such as surrounding paleo-uplifts and paleo-faults. This influence has led to differences in the distribution of sedimentary facies belts between this area and other parts of the Sichuan Basin. Additionally, the Dengying Formation in northeastern Sichuan is characterized by deep burial depth and relatively limited drilling data, which have constrained the accurate acquisition of stratigraphic parameters. Previous studies have predominantly focused on macro-scale, regional sedimentary frameworks [22–24]. Gaps remain, however, including the lack of high-resolution characterization of lithofacies paleogeographic distribution in northeastern Sichuan and the absence of systematic research on the primary controlling factors of sedimentary evolution in this specific region.

In light of the aforementioned research gaps, this study integrates data from field outcrops, drill cores, and well logging to conduct sedimentary forward modeling of the Dengying Formation in the northeastern Sichuan Basin using DionisosFlow 2017. Leveraging a sensitivity analysis approach, we investigate the impacts of various factors on sedimentary evolution in depth, with the aim of establishing a sedimentary evolution model that better aligns with the actual geological conditions of northeastern Sichuan. This model is intended to provide more precise geological support for hydrocarbon exploration of the Dengying Formation in this region—particularly to achieve breakthroughs in the prediction of favorable sedimentary facies belt distribution.

2. Geological Setting

The Sichuan Basin constitutes a large cratonic superimposed basin. Regionally, the Sichuan Basin delineates distinct tectonic zonation: eastern Sichuan is characterized by high-steep fold belt, northern Sichuan by low-gentle structural domain, central Sichuan by a flat-lying structural belt, western Sichuan by a low–steep structural segment, southwestern Sichuan by a low-fold structural belt, and southern Sichuan by a low–steep domal belt, a pattern tightly linked to the late Ediacaran tectono-sedimentary evolution of the basin. Post Dengying deposition, the Caledonian paleo-uplift in the Sichuan Basin underwent roughly five tectonic evolution stages—the early Caledonian cycle, in particular, witnessed two tectonic episodes: Tongwan Episode I and Tongwan Episode II [25]. During the Dengying Formation sedimentary interval, a stable carbonate platform regime prevailed across the basin overall—a setting shaped by regional tectonic quiescence during the Ediacaran. Tectonically, this carbonate platform was subjected to multi-episode differential crustal uplift linked to the Tongwan Movement, an influence that triggered the regional development of two unconformity surfaces. These key surfaces lie at the tops of the Dengying Formation's second member and fourth member. What role did these unconformities play in shaping the basin's stratigraphic architecture? They serve as critical markers for sequence division and paleogeographic reconstruction.

Stratigraphically, Deng-2 Member maintains an unconformable contact with the overlying third member (Deng-3 Member) of the Dengying Formation, whereas Deng-4 Member forms an unconformable boundary with the overlying Qiongzhusi Formation. Leveraging the top Deng-2 and top Deng-4 unconformities as sequence boundaries, and incorporating insights from prior investigations [26,27], the Dengying Formation is subdivided into two third-order sequences. Termed ZSQ1 and ZSQ2 in ascending stratigraphic order, these sequences encapsulate the basin's sedimentary evolution during the late Ediacaran.

The study area lies in the northeastern Sichuan Basin, stretching 271 km east–west and 306 km north–south (Figure 1a). Vertically, the Upper Sinian Dengying Formation within this area is subdivided into four members in ascending order: Deng-1 Member (abbreviated), Deng-2 Member, Deng-3 Member, and Deng-4 Member [28]—a division

consistent with regional stratigraphic correlations. Deng-1 Member formed during the transgressive stage of the early Late Sinian. Its lithological assemblage consists of light gray to dark gray bedded micritic dolomite and silt-sized crystalline dolomite, intercalated with minor stromatolitic dolomite. Deng-2 Member is dominated by light gray to grayish white thrombolitic dolomite and silt-sized crystalline dolomite. Thrombolitic fabrics, stromatolitic fabrics, and laminitic fabrics are well developed, with multiple layers of superimposed grape lace structures visible. Deng-3 Member's main lithologies are dark gray to gray dolomitic siltstone and dolomitic mudstone. Deng-4 Member comprises light gray to gray bedded silt-sized crystalline dolomite, intraclastic dolomite, and algal dolomite. Locally, siliceous dolomite and chert are observed (Figure 1b).

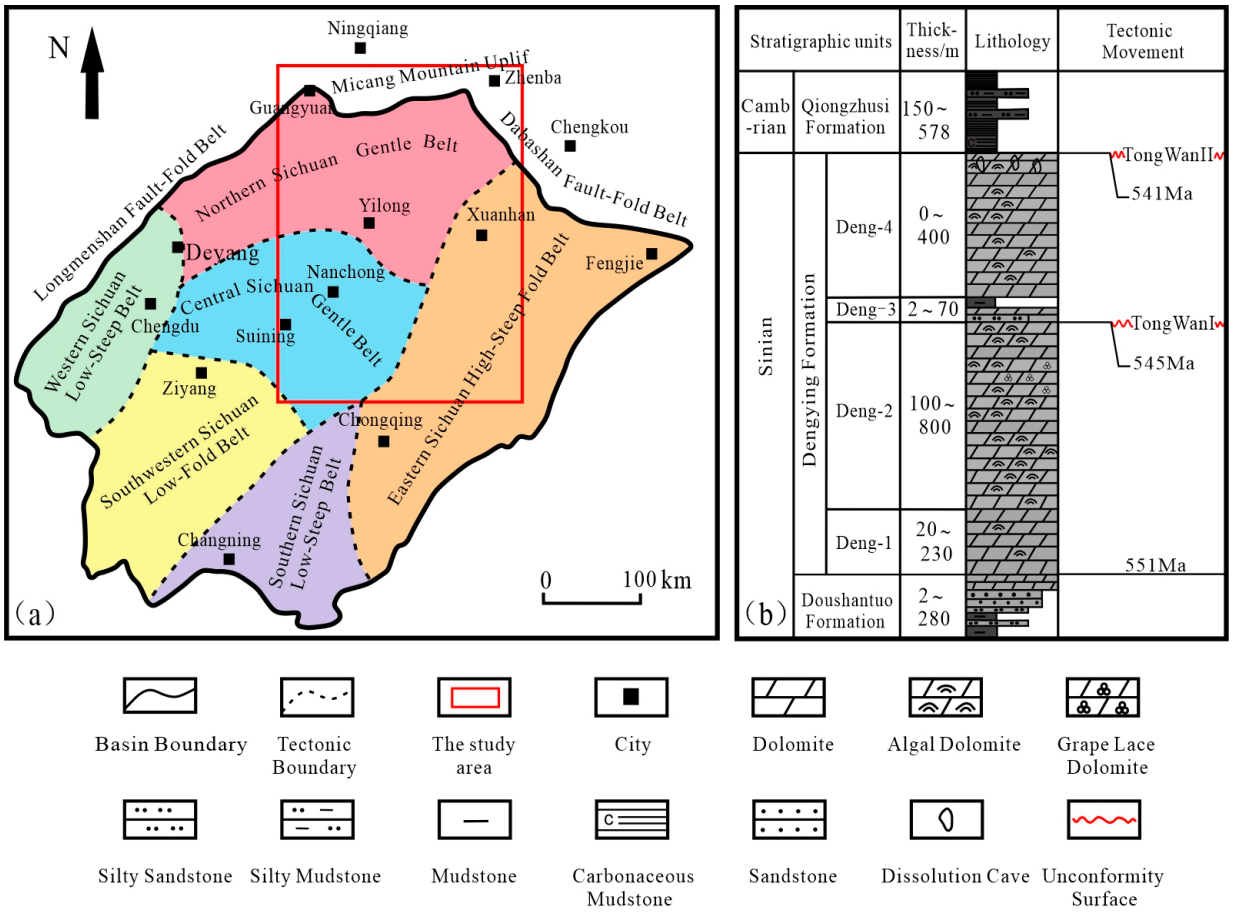


Figure 1. Comprehensive columnar section of tectonic location and Dengying Formation in study area. (**a**) Major tectonic divisions and location of study area in Sichuan Basin. (**b**) Stratigraphic lithology and characteristics.

3. Methods

3.1. Types of Sedimentary Facies

The Nanjiang Yangba section was measured in situ; samples were collected and thin sections prepared thereafter in Nanjiang, China. Meanwhile, cores were examined at the Daqing Oilfield Core Repository, and logging data were collated and systematically organized. Building on the aforementioned datasets and previous sedimentary facies classification schemes [29], this study integrates observations from extensive field outcrop sections and drill cores. Based on lithological characteristics—including color, bed thickness, and sedimentary structures—and combined with vertical lithological assemblage patterns, the dolomite sedimentary facies of the Dengying Formation in the northeastern

Sichuan Basin are primarily classified into two facies: platform margin and restricted platform. Further subdivision identifies four subfacies: microbial (algal) mound, grain shoal, intershoal sea, and intraplatform depression (Table 1).

Table 1. Main sedimentary facies types and identification characteristics in northeastern Sichuan Basin.

Subfacies Type	Lithology	Sedimentary Structure	Logging Response	Typical Well Location/Profile
Microbial (algal) mound	algal dolomite, stromatolite dolomite, thrombolite bonded dolomite, grape lace dolomite	algal lamina structure, grape lace structure	low natural gamma-ray values with a serrated box shape	Gaoshi 1 well, Tianxing 1 well, Nanjiang Yangba
Grain shoal	sand lithic dolomite, gravel lithic dolomite, oolitic dolomite, dissolved pore dolomite	bird-eye structure, vuggy structure	medium–low natural gamma-ray values, showing a serrated box or bell shape	Gaoshi 1 well, Tianxing 1 well, Nanjiang Yangba well, Mashen 1 well
Intershoal sea	(containing) sandy dolomite, micritic dolomite, argillaceous dolomite	horizontal bedding	medium–high natural gamma-ray values, medium–low resistivity values, with serrated logging curves	Mashen 1 well, Nanjiang Yangba
Intraplatform depression	mud crystal dolomite, siliceous dolomite	horizontal bedding	high natural gamma-ray values, high resistivity values, with gently serrated logging curves	Wutan 1 well

3.1.1. Microbial (Algal) Mound

The dominant lithologies of the microbial (algal) mound subfacies include algal dolomite, stromatolitic dolomite, thrombolitic boundstone dolomite, and botryoidal lace dolomite (Figure 2a–d). Field outcrop observations and microscopic thin-section analyses reveal well-developed algal laminae (Figure 2a) and grape lace structure (Figure 2d). The grape lace structure is a distinctive type of concentric encrusting cement fabric. In plan view, it appears as hemispherical protrusions with diameters of several millimeters to centimeters, resembling clusters of grapes, and is densely distributed within the pores or vugs of algal dolostone. In cross section, it displays evenly thick concentric laminae stacked layer upon layer, similar to delicate lace, thus giving rise to its full name: the "grape lace" structure. It occurs mainly in dissolution pores, vugs, and fractures of algal dolostone in the Second Member of the Dengying Formation, growing symmetrically inward to form framework-like or banded textures, and is commonly filled with sparry dolomite or bitumen. The laminae formed by algal growth appear as alternating layers of varying colors and thicknesses, exhibiting distinct rhythmicity; this represents one of the key diagnostic markers for identifying microbial mounds. On well logs, the microbial (algal) mound subfacies is characterized by low natural gamma (GR) values, with an overall serrated box-shaped log response. In drill cores, irregular massive structures and pores formed by algal binding are visible, and bioturbation traces can be observed locally. Due to the binding and trapping effects of organisms on sediments during growth, geobodies with a certain hydrodynamic resistance—typically mound-like or lenticular in shape—are formed. Consequently, microbial mounds are predominantly developed in platform margin settings, and their formation usually indicates a depositional environment with relatively strong hydrodynamic energy.

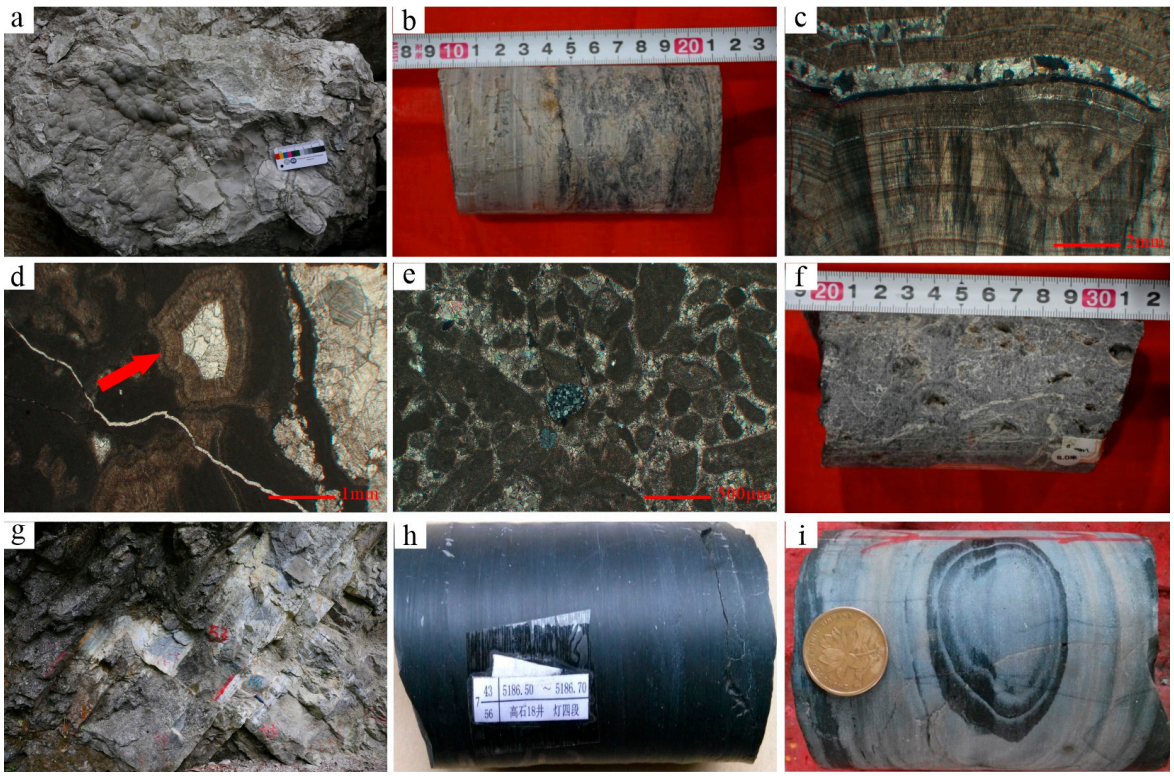


Figure 2. Outcrop, core, and thin section images of main subfacies in the study area. (**a**) Botryoidal lace dolomite, Deng-2 member, NanjiangYangba; (**b**) algal laminated dolomite, Deng-4 member, 5575.30~5575.41 m, Heshen 2 well; (**c**) stromatolite dolomite, Deng-2 member, Nanjiang Yangba; (**d**) grape lace structure, Deng-2 member, Nanjiang Yangba; (**e**) sparry intraclastic gravel dolomite, Deng-2 member, Nanjiang Yangba; (**f**) dissolved pore dolomite, 5590.90~5591.10 m, Heping 1 well; (**g**) thin middle-layer micritic dolomite with thin-layer argillaceous dolomite above the grape lace structure development section, Deng-2 member, Nanjiang Yangba; (**h**) black micritic dolomite, Deng-4 member, 5186.50~5186.70 m, Gaoshi 18 well; (**i**) micritic dolomite with siliceous mass, Deng-4 member, 5181.65~5181.73 m, Gaoshi 18 well.

3.1.2. Grain Shoal

The grain shoal subfacies is dominated by lithologies such as sandy (gravelly) clastic dolomite, oolitic dolomite, brecciated dolomite, and dissolved-pore dolomite. These lithologies typically exhibit good sorting and roundness (Figure 2e). On well logs, the grain shoal subfacies is commonly characterized by medium to low natural gamma (GR) values, with a log response morphology of a serrated box shape or bell shape. Drill core observations reveal the development of grain dissolution pores (Figure 2f). Driven by hydrodynamic processes (e.g., waves and tides) that transport and redeposit sediments, the grain shoal subfacies is predominantly developed in the platform margin zone and intraplatform topographic high. These characteristics indicate that it was deposited in a shallow subtidal high-energy environment—between mean low tide and wave base—where hydrodynamic conditions were strong and influenced significantly by tidal and wave activity.

3.1.3. Intershoal Sea

The intershoal sea subfacies is primarily composed of micritic dolomite; locally, argillaceous dolomite forms due to high argillaceous content. Vertically, this subfacies exhibits lithological variations, including micritic dolomite, argillaceous dolomite, their transitional types, and interbedding of these lithologies (Figure 2g). On well logs, it is characterized by serrated medium-to-high natural gamma (GR) values and high resistivity values. Key diagnostic features of this subfacies include gray to dark gray coloration, horizontal bedding, and

relatively large cumulative thickness (Figure 2h)—all indicative of deposition in a quiescent water environment below the fair-weather wave base. Vertically, the intershoal sea subfacies alternates with the microbial (algal) mound and grain shoal subfacies, further confirming that it formed in topographically low-lying areas with weak hydrodynamic conditions.

3.1.4. Intraplatform Depression

Lithologically, the intraplatform depression subfacies is similar to the intershoal sea subfacies, being dominated by micritic dolomite; locally, high silicification leads to the formation of siliceous dolomite (Figure 2i). Drill cores exhibit a dark color (gray to dark gray) with visible horizontal bedding. On well logs, this subfacies is characterized by high natural gamma (GR) values and high resistivity values. Compared with the intershoal sea subfacies, the micritic dolomite and siliceous dolomite of the intraplatform depression subfacies have a greater vertical superimposed thickness—often forming lithological intervals exceeding 50 m. This feature indicates deposition in a stable low-energy environment between mounds and banks. Based on this observation, the continuous, thick-bedded (siliceous) micritic dolomite is independently defined as the intraplatform depression subfacies, which marks the low-lying areas between mound and grain shoal within the carbonate platform.

3.2. Simulation Design and Data

Sedimentary forward modeling conducted on the Dionisos software platform enables the reconstruction of stratigraphic sedimentary filling processes and lithological distribution across four dimensions—three spatial dimensions (3D) and one temporal dimension [30–34]. The input parameters for carbonate sedimentary forward modeling primarily fall into four categories. Deterministic fundamental parameters, including the size of the simulated study area, time scale and time step, simulation grid resolution, and lithology types. The second is accommodation space-influencing parameters. This category comprises initial paleowater depth, tectonic subsidence of the basin basement, and relative sea level changes. These parameters exert a significant impact on the variation in accommodation space within the simulated study area. The next category is carbonate production rate, a critical parameter governing the accumulation rate of carbonate sediments, directly influencing the thickness and distribution of carbonate deposits. Wave parameters include the range of wave influence and wave depth, which regulate hydrodynamic conditions and sediment transport/deposition patterns in the simulated system.

3.2.1. Basic Parameters

This study aims to analyze the distribution and location of sedimentary facies. It is necessary to consider the relationship between simulation accuracy and simulation time, and to define the basic data of the basin, including geometry, time, and lithologies. The simulated study area is commensurate in size with the actual research domain. The basin size is defined as 270 km × 300 km, the grid spacing is 10 km (27 × 30 grid), and the initial basement thickness is 20 m. The simulation time is set from 551 Ma to 541 Ma [35], encompassing a total of 10 Myr with a 0.5 Myr time step. Carbonate lithology, notably, is tightly coupled to reef and algal productivity; combined with the types and characteristics of the sedimentary facies mentioned above, five main types of carbonate facies are defined, namely ‘mound’, ‘shoal’, ‘intershoal sea’, ‘intraplatform depression’, and ‘mud’. The bioherm represents a high-energy environment, the grain shoal represents a relatively high-energy sedimentary environment, the intraplatform depression and the intershoal sea represent a relatively low-energy sedimentary environment, and the mud represents a deep-water sedimentary environment.

3.2.2. Initial Bathymetry Map

The paleotopography (initial basement topography) at the beginning of sedimentation in northeastern Sichuan is a very critical input parameter. When sedimentary forward modeling is carried out, the initial geomorphological form should be determined first, and then the simulation should be carried out on this basis. The conventional method of setting the initial water depth map is to convert the bottom structure map into a paleogeomorphologic map (Figure 3), and on this basis, the ancient water depth is judged according to the distribution characteristics of sediments. The late tectonic action in the Xuanhan–Kaijiang area is strong, which may be caused by the dislocation of faults, and the conventional method of setting ancient water depth is not accurate. Finally, using the paleogeomorphology trend combined with the sedimentary environment, we can analyze the initial water depth (Table 2) based on the concept of the high sensitivity of carbonate rock types to water depth and wave energy (Figure 4).

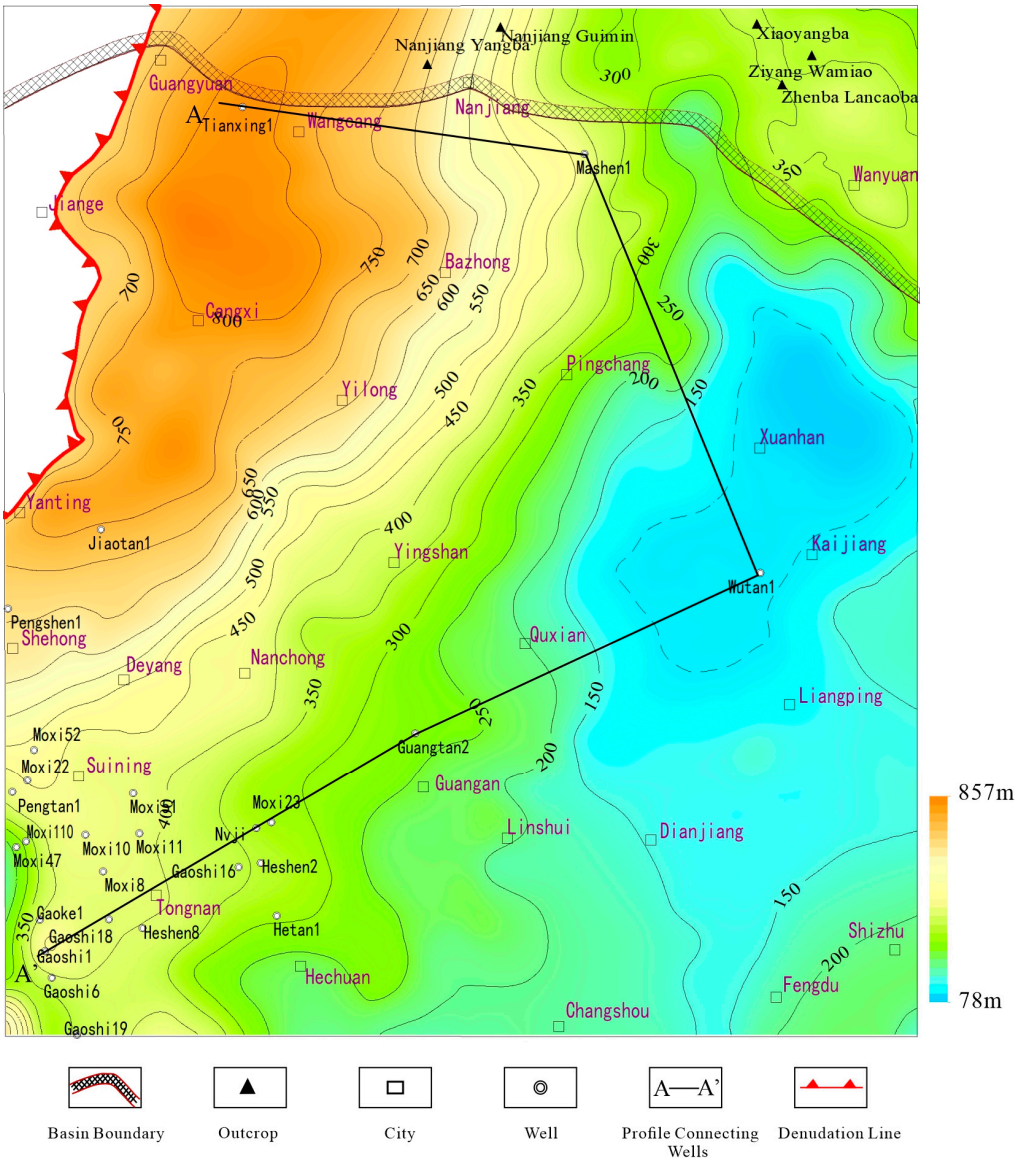


Figure 3. A paleogeomorphic map of the Dengying Formation in the northeastern Sichuan Basin.

Table 2. Sedimentary facies/lithofacies subdivisions of Dengying Formation constrained by paleowater depths and lithologies. (Modified from [21,36,37].)

Sedimentary (Sub) Facies/Lithofacies	Assignment Principle
Microbial (algal) mound	Between mean low tide and mean high tide, with water depth ranging from 5 to 10 m.
Grain shoal	From mean low tide to near wave base, with water depth ranging from 10 to 25 m.
Intershoal sea	Below the microbial mounds on the inner side of the platform margin, with water depth ranging from 25 to 35 m.
Intraplatform depression	Located in the low-lying area between mound–shoal complexes, the water depth is slightly deeper than that of intershoal sea, with water depth ranging from 35 to 50 m.
Slope-Basin	Water depth greater than 50 m.

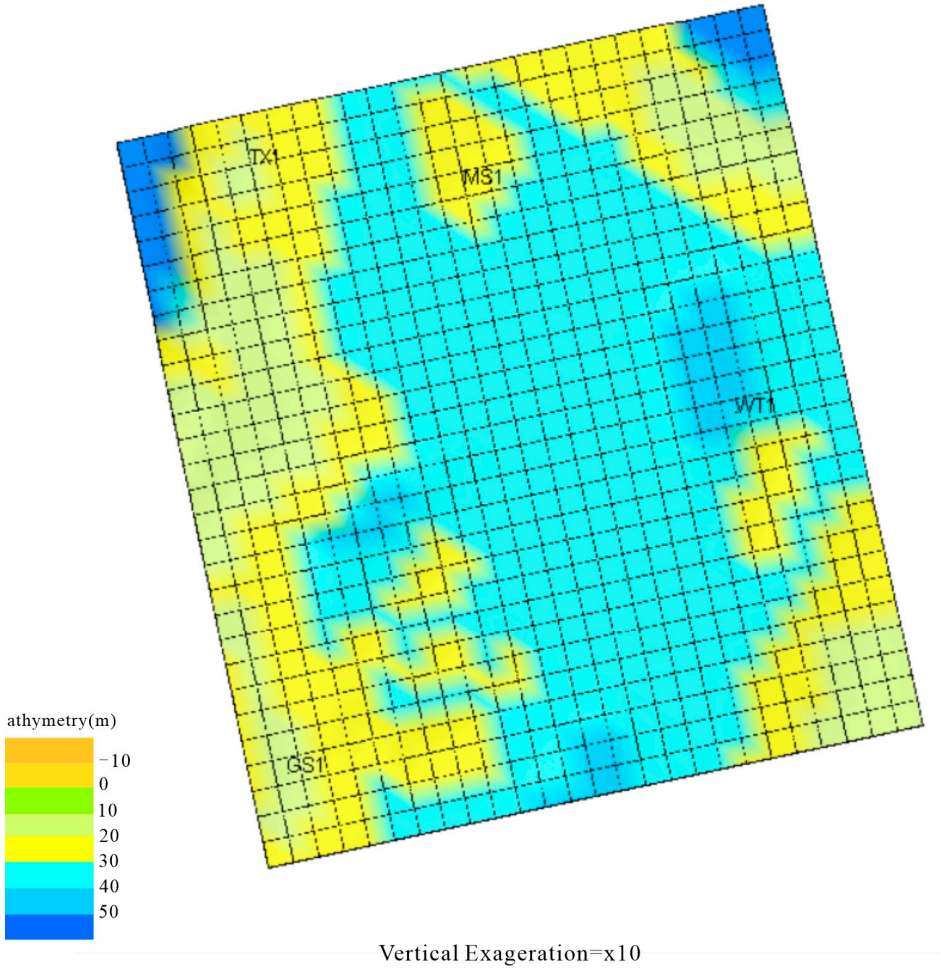


Figure 4. Initial paleowater depth map of study area.

3.2.3. Eustasy

Relative sea level changes regulate seawater depth while modulating sedimentary accommodation space—two interlinked effects that underpin carbonate development. Therefore, relative sea level change plays a pivotal role in the development of carbonate strata. In this study, the sea level change curve is defined according to the relative sea level change of the simulated work area. By analyzing the cyclic changes in the Gaoshi 1 well in the working area, it is identified that the sea level in the simulated working area follows

a rising and falling curve that rises rapidly and then decreases slowly, and this curve is superimposed by seven stages of quasi-sequences that rise first and then fall (Figure 5).

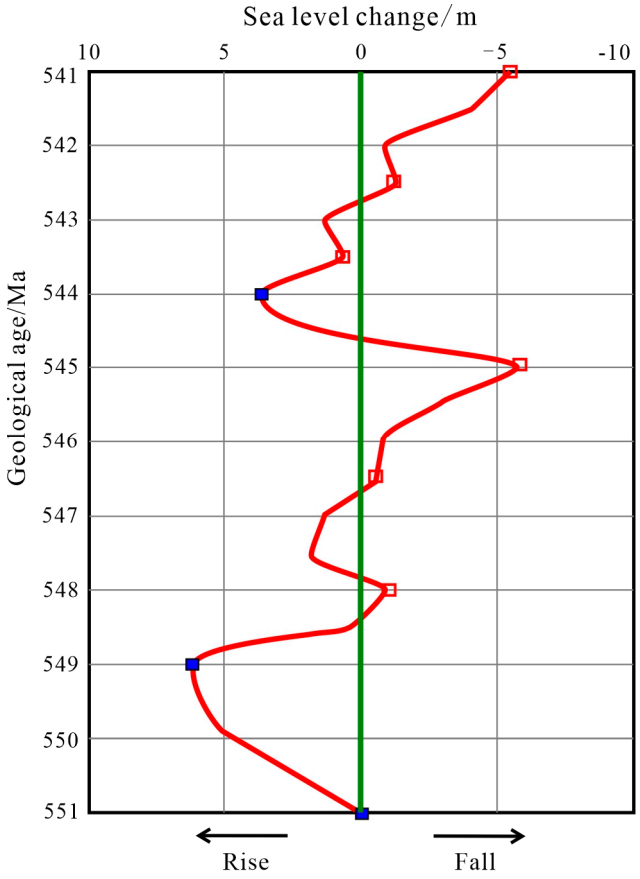


Figure 5. Sea level change curve in study area. The green line represents a horizontal level change of 0. The red line represents sea level change.

3.2.4. Subsidence

Structural subsidence stands as another dominant control on sedimentary accommodation space—one that operates in tandem with relative sea level changes to modulate carbonate deposition. Unlike sea level fluctuations that alter water depth directly, subsidence adjusts the vertical capacity for sediment accumulation, a distinction critical to interpreting the Ediacaran Dengying Formation's stratigraphic architecture. The thickness of the Dengying Formation was corrected by ancient water depth correction and decompaction recovery. At the same time, the total settlement was obtained by referring to a previous study [38]. Taking this as the initial value, the simulation was preliminarily carried out. The simulation results were repeatedly corrected and iterated with the actual well and seismic data to obtain the most reasonable structural settlement input data (Table 3).

Table 3. Subsidence amount of the Dengying Formation in the study area.

Time (Ma)	Average Value (m)	Maximum Value (m)	Minimum Value (m)
541	42.9	85.6	13.3
542	38.3	81.5	8.7
543	37.6	78.5	8.9
544	36.4	76.9	7.4
545	41.9	84.7	12.8
546	37.7	80.5	8.2

Table 3. *Cont.*

Time (Ma)	Average Value (m)	Maximum Value (m)	Minimum Value (m)
547	36.9	77.2	7.7
548	38.1	81.3	8.6
549	32.8	72.6	5
550	34.4	74.2	6.7
551	0	0	0

3.2.5. Carbonate Productivity

In the study of paleogeographic reconstruction of carbonate sedimentary systems in geological history, it is hard to accurately estimate the rate of carbonate accumulation. The vertical growth rates of different sedimentary facies units were determined by constructing a 'carbonate production rate–time step' coupling model [39–41]. Based on previous studies [21], the Dengying Formation is subdivided into 5~9 lithofacies types, and five types of carbonate facies are summarized. The fuzzy logic relationship between the growth of five types of carbonate rocks and the depth of the water body is established (Table 4), which is transformed into input parameters, and finally the relationship between carbonate rock yield and water depth is obtained (Figure 6).

Table 4. Relationship between various carbonate productivity and water depth values.

Water Depth (m) \ Lithofacies	Mound	Shoal	Intraplatform Depression	Intershoal Sea	Mud
0	0	0	0	0	0
5	1	0	0	0	0
7.5	1	0	0	0	0.1
10	1	0	0	0	0.14
12.5	0.9	1	0	0	0.22
15	0.85	1	0	0	0.3
17.5	0.74	1	0	0	0.41
20	0.68	0.8	0	0.2	0.5
22.5	0.5	0.6	0	0.6	0.55
25	0.35	0.55	0	0.8	0.7
27.5	0.2	0.5	0.2	1	0.75
30	0	0.4	0.4	1	0.8
32.5	0	0.33	0.62	0.85	0.85
35	0	0.25	0.79	0.57	0.9
37.5	0	0.14	1	0.2	1
40	0	0.08	1	0	1
42.5	0	0	0.65	0	1
45	0	0	0.4	0	1
47.5	0	0	0.16	0	1
50	0	0	0	0	1

Variations in water depth and wave energy exert a significant impact on carbonate productivity—meaning it is essential to define parameters that govern how carbonate yield varies with these two key environmental factors. Among them, water depth is the first important factor affecting the yield of carbonate rocks. With the evolution of time, the yield of carbonate rocks usually decreases with water depth, and most of them change exponentially. Therefore, it is necessary to define not only the relationship between carbonate rock yield and water depth, but also the relationship between carbonate rock yield and time. The relationship between carbonate rock yield and time is defined by absolute growth yield, that is, the growth rate per unit time. Taking into account the high

yield of mounds and grain shoals, the yield is set to 80 m/Myr and 60 m/Myr, respectively, the intershoal sea is set to 40 m/Myr, the depression is set to 20 m/Myr, and the mud yield is very low, set to 1 m/Myr.

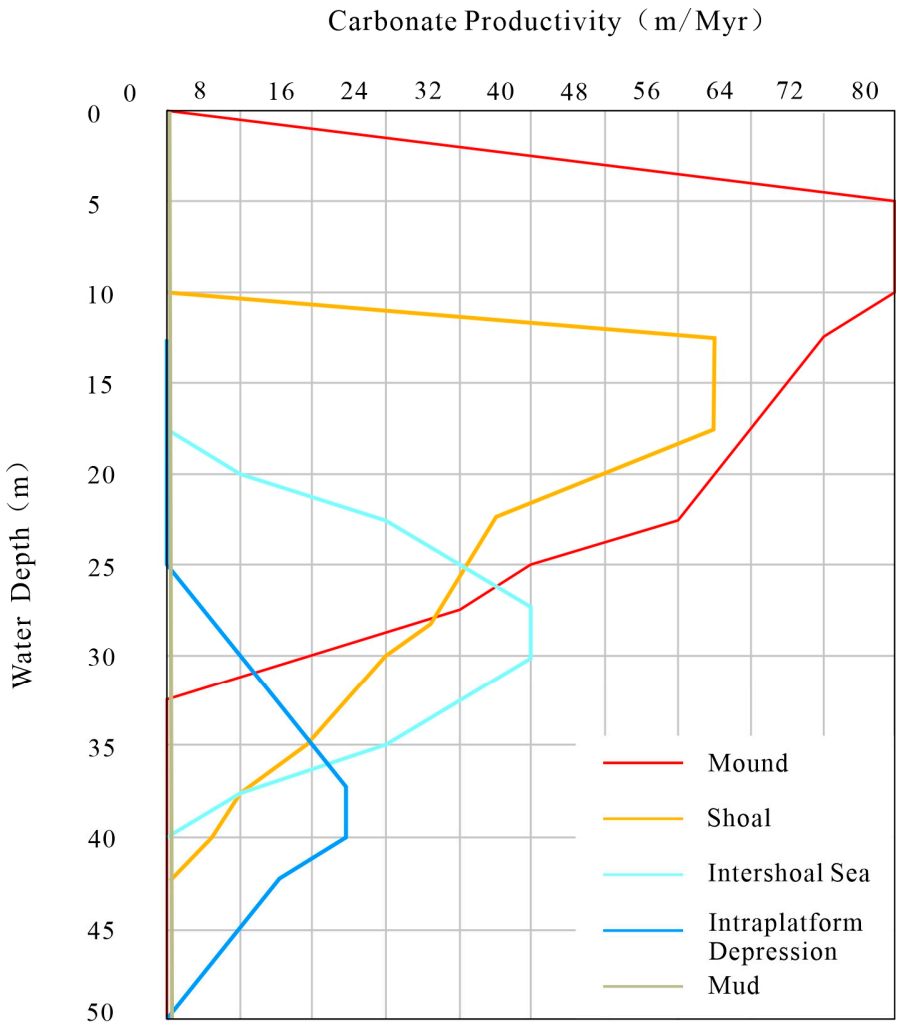


Figure 6. Carbonate productivity map.

3.2.6. Wave Parameter

Another important factor affecting the yield of carbonate rocks is wave energy. When the wave energy is too strong, it will cause the mound to be eroded. To differentiate carbonate productivity across diverse depositional environments, wave energy sensitivity and wave parameters need to be defined and calibrated. The sensitivity of wave energy is defined by setting the relationship between wave energy and carbonate rock yield. The higher the wave energy, the greater the sensitivity of the wave energy. Mounds and shoals are formed in an environment with high wave energy, and they are set in a higher range. On the contrary, the mud is set within a very low range.

In this paper, two environments are defined based on a wave energy threshold of 30 kW/m (about 10% of the maximum). The high-energy marine environment is the area where the wave energy in the basin is greater than 30 kW/m, and the low-energy environment is the area where the wave energy in the basin is less than 30 kW/m. Therefore, the relationship between wave energy and productivity is defined, and the range of productivity of each lithology is obtained (Table 5).

Table 5. Table of yield ranges for various lithofacies.

Lithofacies	Mound	Shoal	Intraplatform Depression	Intershoal Sea	Mud
Wave Energy (KW/m)	100/10,000	50/10,000	0/50	0/30	0/10
Drift Energy (KW/m)	10/1000	5/1000	0/5	0/3	0/1
Tolerance (%)	0	0	0	0	0

The wave parameters are mainly set by the number, the direction of wave propagation, the depth of action, and the frequency. In this paper, the setting of wave parameters mainly considers the propagation direction and action depth of waves, which mainly affects the energy intensity of carbonate rocks at various positions on the platform and ultimately controls the distribution of different types of carbonate rocks on the platform. It affects the distribution of medium–high energy carbonate rocks, especially microbial rocks.

During the deposition of the Dengying Formation, the Yangtze plate was mainly affected by the southeast monsoon climate from South Asia and Australia [42,43]. Because the area was controlled by the southeast wind field, the wave parameters are optimized by repeated simulation and result feedback. The waves in the two main directions of north (azimuth of 15°) and west (azimuth of 270°) are set, and the wave reference depth, wave propagation angle, and storm frequency are defined (Figure 7).

Number of Waves	Wave A	Wave B
Action Depth (m)	20.0	10.0
Propagation Angle (°)	270	15
Frequency (%)	100	60
Wave Energy (KW/m)	272.8	48.2
Wind Speed (km/h)	61.0	41.0
Wave Period (s)	6.8	4.8
Wave Height (m)	7.2	3.6

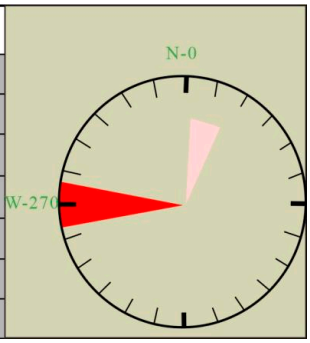


Figure 7. The wind wave propagation angle in the study area.

3.3. Sedimentary Forward Modeling Results and Analysis

The results of sedimentary forward modeling are uncertain, and it is necessary to adjust the simulation parameters many times to achieve consistency between the simulation results and the actual drilling formation thickness, lithology distribution, and other data [32,44]. The reliability of the simulation results is mainly verified by matching the simulation results with the sedimentary facies obtained from the analysis of field outcrops, cores, logging data, and single-well facies.

3.3.1. Verification of Single Well

Gaoshi 1 well resides in the platform margin of the study area's southwestern sector, and two parasequence sets are mainly developed, ZSQ1 and ZSQ2. ZSQ1 preserves a complete transgressive–regressive sedimentary cycle from base to top. Lower intervals are thin-bedded, dominated by micritic dolomite and argillaceous dolomite. Upper intervals thicken substantially, lithologically dominated by granular dolomites (sandy dolomite, brecciated dolomite, etc.) interspersed with minor argillaceous dolomite. ZSQ2 exhibits clear vertical sedimentary differentiation. Its lower segment consists of tidal flat sedimentary cycles, thin-bedded and typified by argillaceous dolomite and micritic dolomite. The upper part features thin-bedded intershoal micritic dolomite, alongside massive mound–shoal complex deposits. These complexes are predominantly composed of granular dolomite,

with subordinate algal dolomite—an indicator of high-energy depositional conditions during regression. This vertical lithofacies variation directly records shifts in paleowater depth and energy regimes across transgressive–regressive cycles, consistent with platform margin sedimentary processes in the Ediacaran.

Comparing the simulated well GS1 with the single-well sedimentary facies of Gaoshi 1 well (Figure 8), the actual drilling is consistent with the simulated well sequence, indicating that the simulation results in this well area are correct.

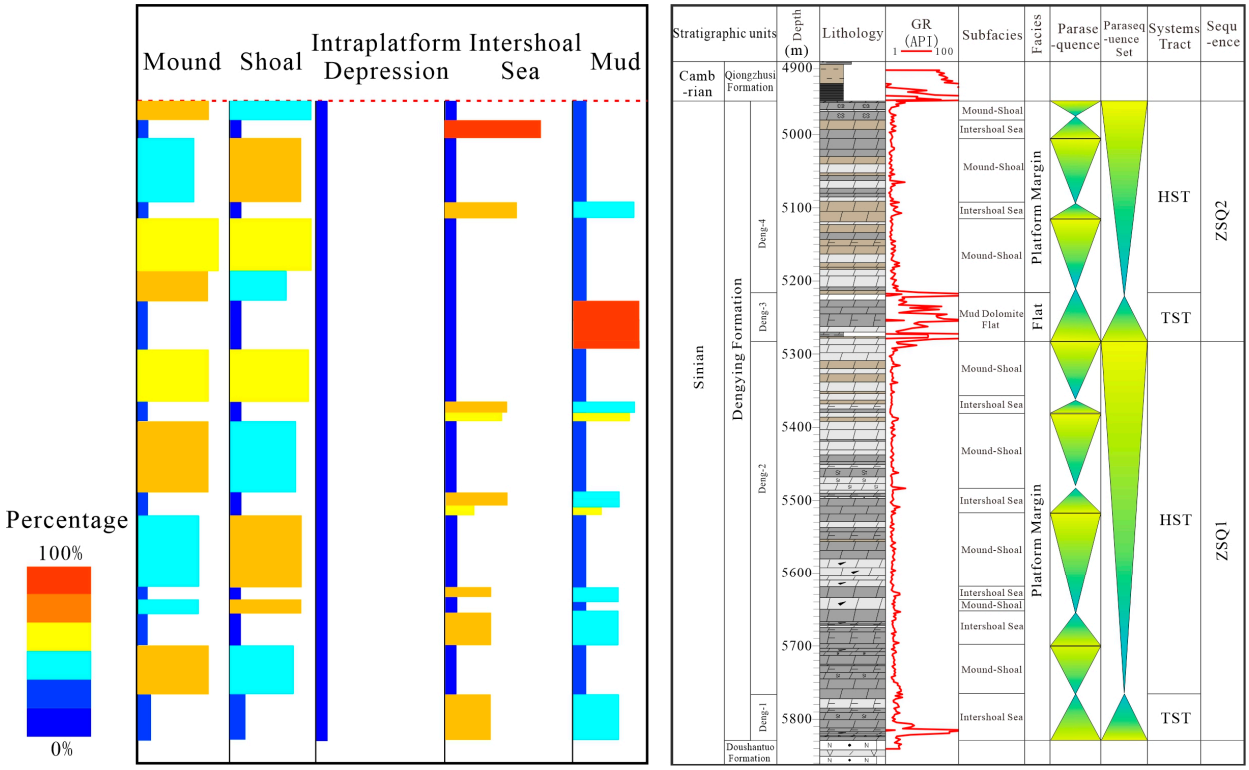


Figure 8. Comparison of sedimentary facies between simulated well GS1 and actual drilled well Gaoshi 1.

3.3.2. Plane Distribution of Sedimentary Facies

Comparative analysis of the simulated sedimentary facies plane distribution map with paleotopographic maps and real relevant geological maps reveals good consistency in their planar distribution. The western and eastern parts of the study area correspond to paleotopographic highs, where microbial mounds and granular shoals overlap to form mound–shoal complexes; the platform margin mound–shoal complexes in the west exhibit a larger distribution range than those in the east. The platform margin mound–shoal complexes are continuously distributed at the edge of the platform, with a large scale, and are distributed in the southwest–northeast direction. The northeastern part of the study area is a low geomorphic unit, and the intraplatform depression is developed at the WT1 position. The intraplatform mound–shoal sediments are widely developed in the central region, showing point-like distribution of intraplatform mound–shoal complexes. Both GS1 and TX1 are situated on the western paleotopographic high, and their planar positions in the simulation results fall within the platform margin zone—an observation validating the consistency of the simulated outcomes with actual geological conditions (Figure 9).

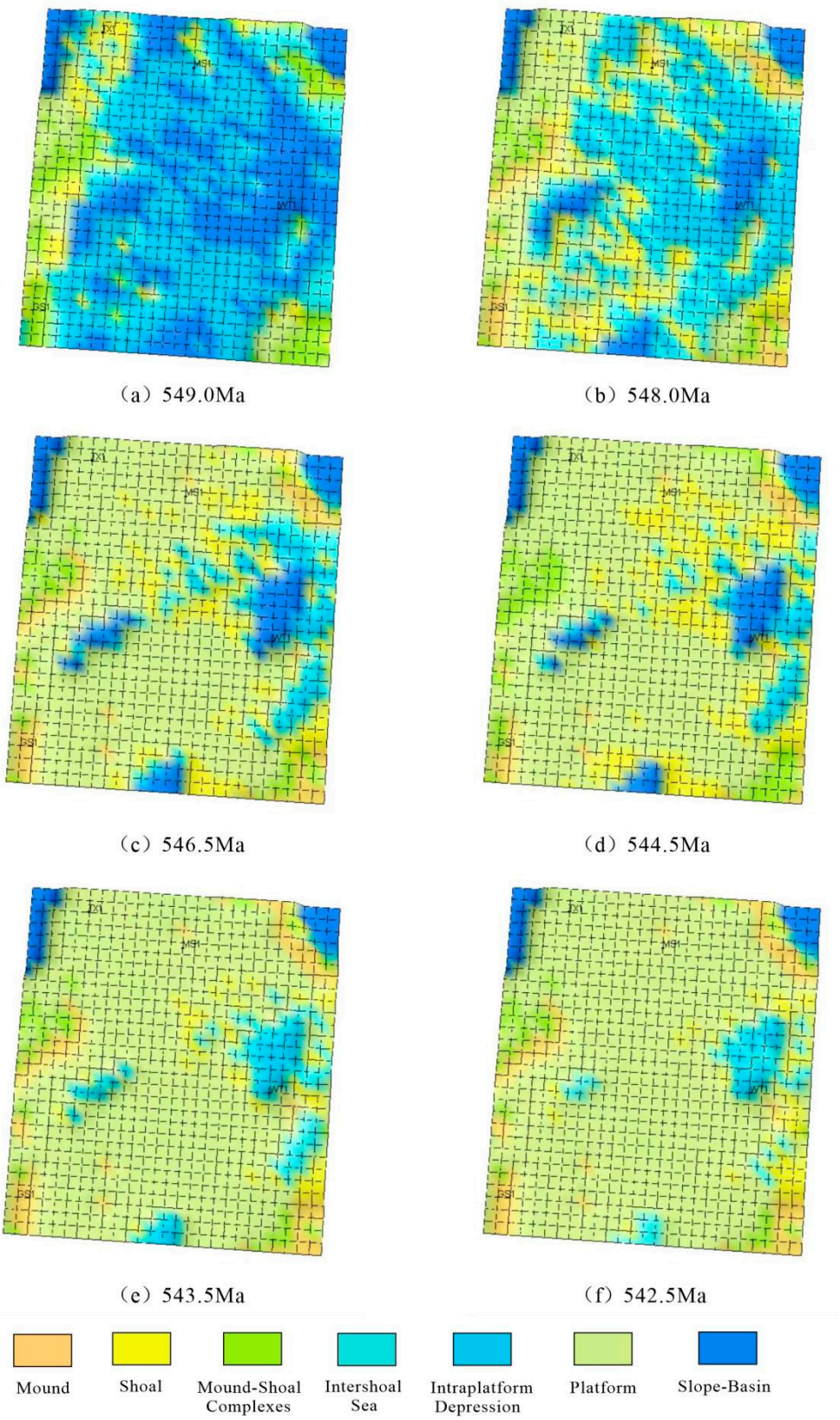


Figure 9. Simulated sedimentary facies distribution maps of the Dengying Formation in the northeastern Sichuan Basin. (**a**) 549.0 Ma simulated sedimentary facies. (**b**) 548.0 Ma simulated sedimentary facies. (**c**) 546.5 Ma simulated sedimentary facies. (**d**) 544.5 Ma simulated sedimentary facies. (**e**) 543.5 Ma simulated sedimentary facies. (**f**) 542.5 Ma simulated sedimentary facies.

4. Results

4.1. Analysis of Connected Well Sedimentary Facies

Based on single-well sedimentary facies analysis, the planar distribution pattern of sedimentary facies was comparatively examined (Figure 10). Tianxing 1 well and Gaoshi 1 well are located on the platform margin, and their formation thickness is much larger than that of Mashen 1 well, Wutan 1 well, and Guangtan 2 well. Microbial (algal) mounds and grain shoals overlap mutually, presenting as mound–shoal subfacies. Mound–shoal complexes along the platform margin are thicker than those in the platform interior, showing a gradual thinning trend from the platform margin toward the platform center. Within the ZSQ1 and ZSQ2 sequences, as sea level fell, mound–shoal complexes became more extensively developed in the second and fourth members of the Dengying Formation—intervals corresponding to high-stand system tracts (HSTs), a distribution pattern tightly linked to regressive depositional dynamics. At the location of Wutan 1 well, the thickness of the formation is obviously reduced, supported by the previous proposal that the intraplatform depression subfacies developed in this area [8,45].

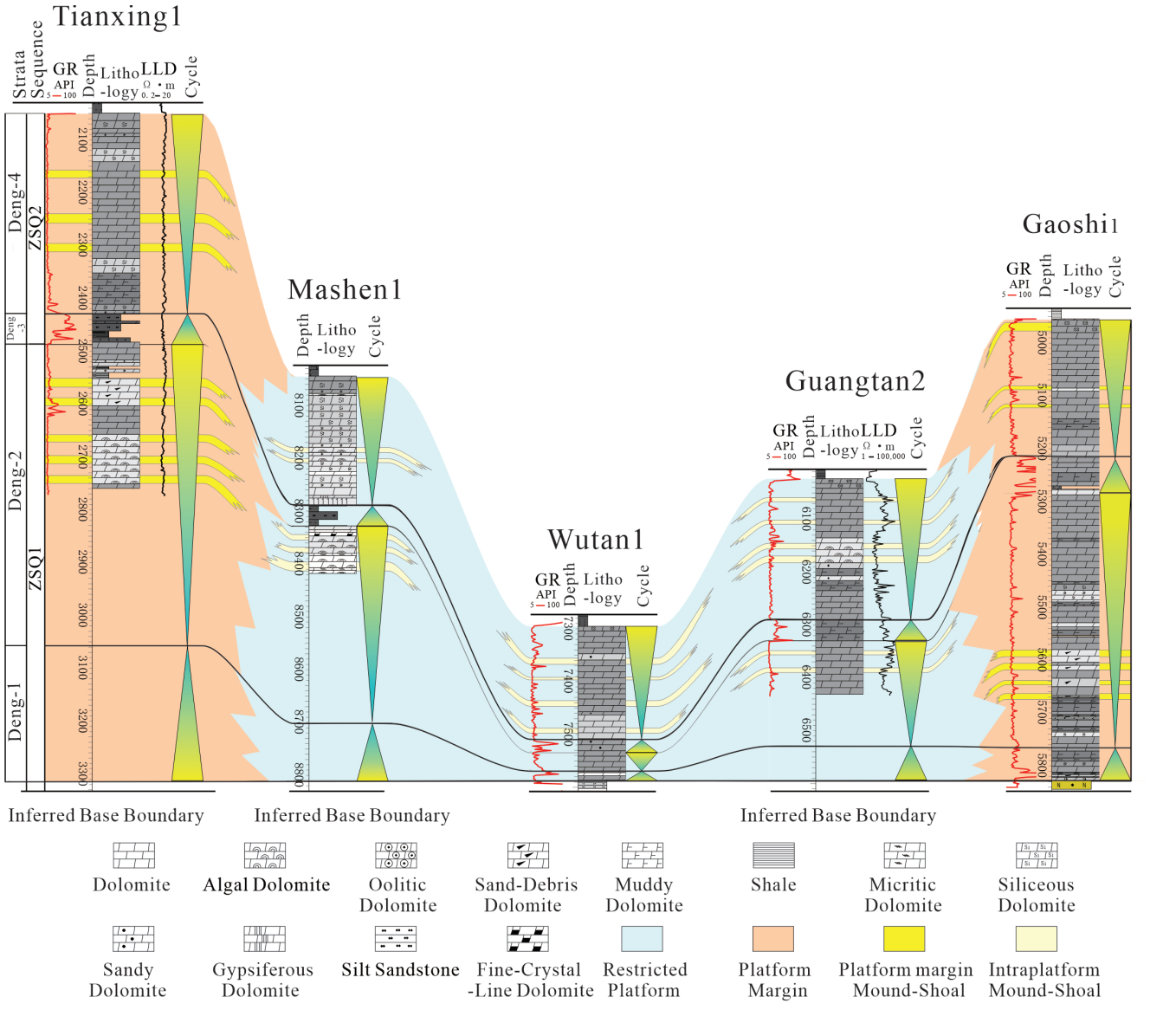


Figure 10. Well-connected sedimentary facies map of Tianxing 1, Mashen 1, Wutan 1, Guangtan 2, and Gaoshi 1 wells in study area (See Figure 3).

4.2. Plane Distribution of Lithofacies Paleogeography

The lithofacies paleogeographic distribution of the Sinian Dengying Formation in the northeastern Sichuan Basin is affected by the paleogeomorphology, and it is still a pattern of uplift and depression on the whole. Based on the data of the core, well logging, seismic, and thin sections, and combined with the results of sedimentary forward modeling (Figure 11a,b), the lithofacies paleogeography of northeastern Sichuan was reconstructed. The lithofacies paleogeographic maps of two third-order sequences of ZSQ1 and ZSQ2 were compiled.

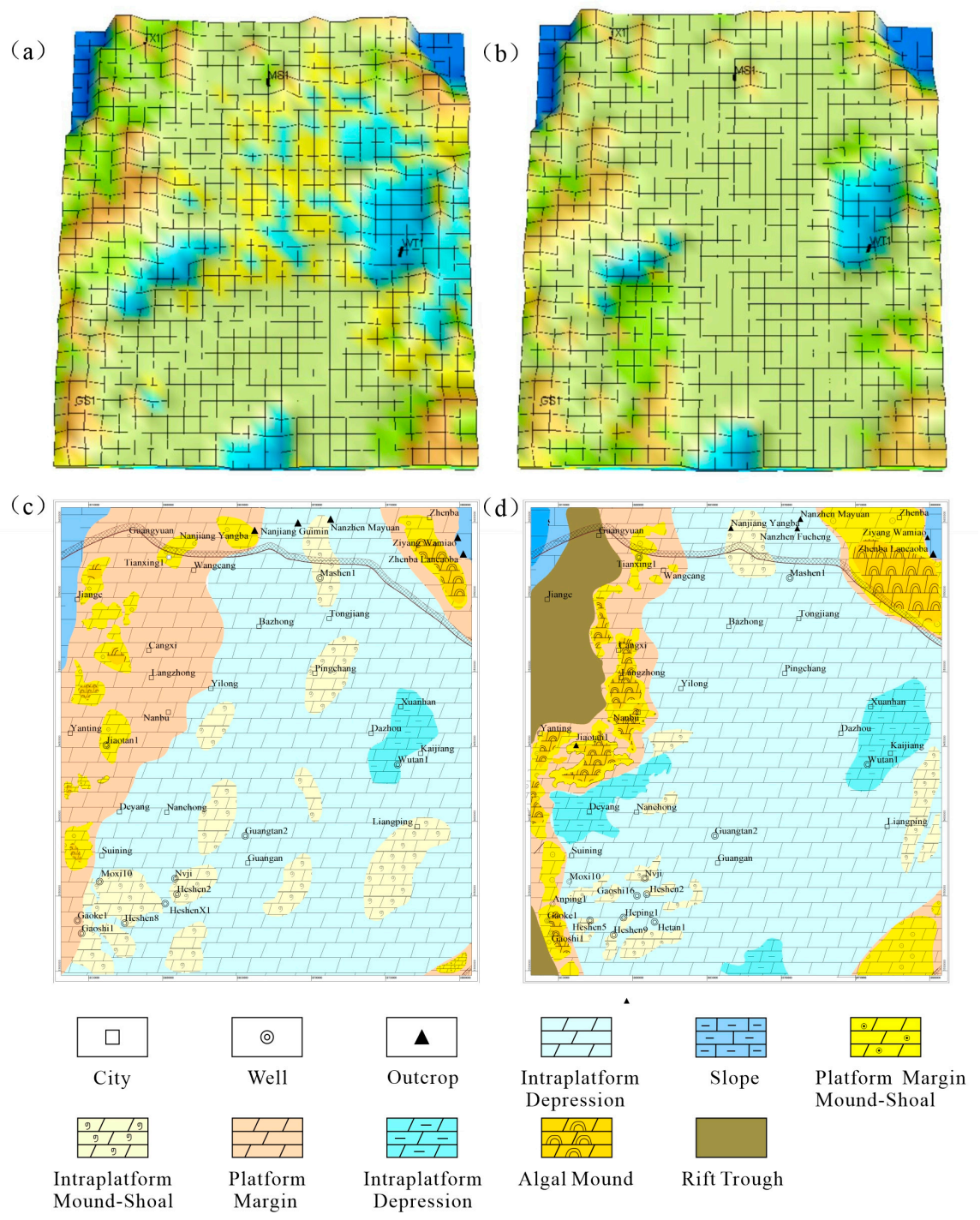


Figure 11. A lithofacies paleogeographic map of the Dengying Formation in the northeastern Sichuan Basin. (**a**) ZSQ1 simulated sedimentary facies. (**b**) ZSQ2 simulated sedimentary facies. (**c**) ZSQ1 lithofacies paleogeographic map. (**d**) ZSQ2 lithofacies paleogeographic map.

During the ZSQ1 period, the western and northeastern sectors of the study area constituted the platform margin, where platform margin mound–shoal complexes were well developed. The eastern main body belonged to the platform interior, with intraplatform mound–shoal complexes developed therein. From the platform margin toward the paleo-uplift, the development degree of mound–shoal complexes gradually diminishes. Overall, the mound–shoal complexes in the platform margin zone exhibit a larger development scale than those in the platform interior—consistent with the aforementioned thickness and distribution trends observed across multiple wells and simulated facies maps (Figure 11c).

During the ZSQ2 period, the lithofacies paleogeographic pattern of ZSQ1 was largely inherited, with intraplatform mounds initiating shrinkage. The western, northeastern, and southeastern sectors served as platform margins, hosting platform margin mounds. The eastern main body remained the platform interior, where intraplatform mound–shoal complexes developed sporadically—with shoal body scales reduced notably. Intraplatform mound–shoal complexes were relatively well developed in the gentle slope area adjacent to the platform margin zone. Generally, platform margin settings favored the development of mound–shoal complexes, which were scarce in the platform interior. Those in the gentle slope near the platform margin, in particular, displayed more robust development—aligning with the overall facies distribution trend of ZSQ2 inheriting yet evolving from ZSQ1 (Figure 11d).

5. Discussion

5.1. Paleogeomorphology Controls the Type of Sedimentary Facies and the Distribution of Lithofacies Paleogeography

The micro-geomorphic characteristics of the platform control the spatial distribution of sedimentary facies [46]. The northeastern Sichuan presents highlands on both sides of the east and west, with platform and depression in the middle, and the input of debris sources in this area is extremely limited. In the platform background where carbonate rocks are dominantly developed, micro-geomorphic differentiation further restricts the formation mechanism and distribution law of subfacies.

The study area as a whole shows the characteristics of a flat platform landform at the top, which can be subdivided into three sub-units: a platform margin topographic high zone, an intraplatform gentle slope zone, and an intraplatform depression zone (Figure 3). Its spatial distribution has a significant correlation with the range of the platform margin zone, restricted platform, and intraplatform depression environment. The platform margin facies is developed in the high zone of the platform margin landform. The platform margin zone hosts abundant microbial (algal) mounds and grain shoals, presented as mutually superimposed mound–shoal assemblages. Restricted platform facies are developed in the gentle zones of the platform interior, where sporadic mound–shoals and intershoal seas are distributed. Intraplatform depression subfacies occur in intraplatform depression zones, trending generally northeast–southwest (NE-SW). The spatial location, development scale, and water depth of each micro-geomorphic unit collectively govern the distribution of lithofacies paleogeography and the development intensity of sedimentary facies. Comparative analysis of micro-geomorphic unit facies distributions and sedimentary simulation results (Figure 12) reveals a strong correlation between the spatial distribution of simulated sedimentary facies and micro-geomorphic characteristics—further validating the regulatory role of micro-topography in sedimentary facies zonation.

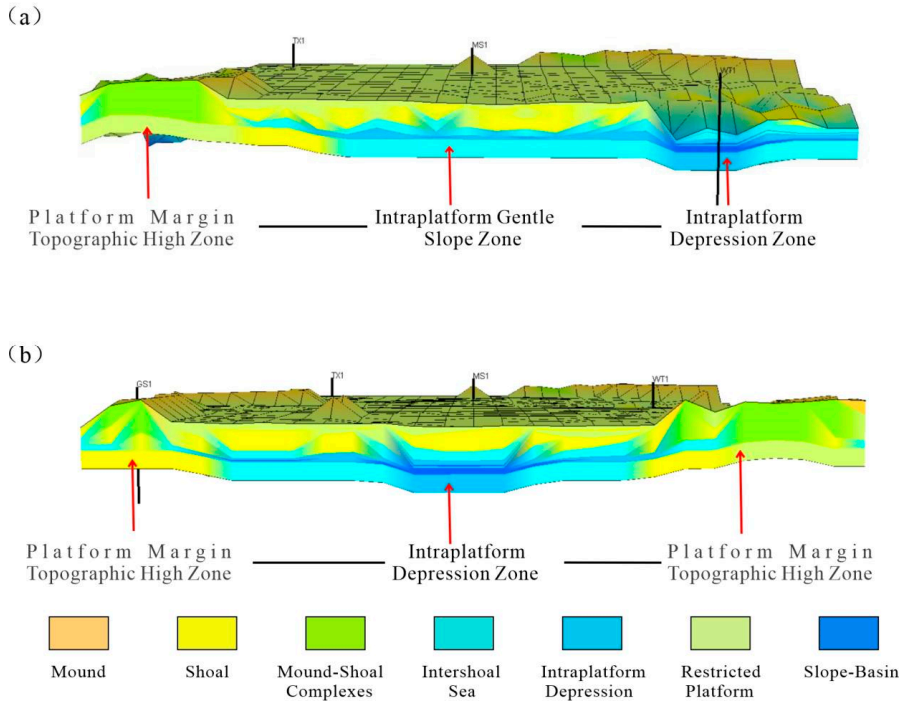


Figure 12. Comparison of simulation results between paleogeomorphology and sedimentary Facies. (**a**) Through east–west section of WT1. (**b**) Through east–west section of GS1.

5.2. Sea Level Change Controls the Development Scale and Lateral Migration of Mound–Shoal Complexes

Sea level fluctuations modulate sedimentary accommodation space, while water depth variations in turn regulate carbonate productivity. Carbonate accumulations in the study area are predominantly enriched within high-stand system tracts (HSTs)—a distribution pattern underscoring the dominant control of sea level changes on marine carbonate development during these intervals. This regulatory mechanism aligns with the aforementioned vertical and planar facies variations, as sea level-driven shifts in accommodation space and water depth directly dictate the growth, accumulation, and preservation of mound–shoal complexes and other carbonate lithologies across the Ediacaran Dengying Formation [47].

Sedimentary cycle analysis reveals that sea level variations of the Dengying Formation in the study area follow a distinct pattern: transgression (sea level rise) during the first and third members, and regression (sea level fall) during the second and fourth members. These variations are encapsulated within two parasequence sets (ZSQ1 and ZSQ2), each comprising multiple stages of water level fluctuation cycles. At 549.5 Ma, sea level peaked—restricting platform margin mound–shoal complex development to small scales, with most of the platform covered by deep waters and dominated by intraplatform depression subfacies (Figure 13a). By 547 Ma, sea level had fallen sharply, triggering large-scale development of mound–shoal complexes across the study area. The platform interior was dominated by extensive mound–shoal complexes and intershoal sea subfacies, with intraplatform depression subfacies limited to local areas (Figure 13b). A brief, rapid sea level rise occurred at 544 Ma, favoring the development of grain shoal subfacies as the dominant facies type in the region (Figure 13c). At 543 Ma, sea level declined slowly, and platform margin mound–shoal complexes were primarily developed in the northern and southern sectors of the margin zone (Figure 13d). Rapid transgression during the first and third members of the Dengying Formation drove sea level rise and increased water depth, which in turn reduced carbonate productivity. Under such conditions, mound–shoal complexes were small in scale and mainly confined to the platform edge. In contrast, slow regression

during the second and fourth members led to sea level fall and decreased water depth, boosting carbonate productivity. This shift promoted larger-scale development of mound–shoal complexes, which gradually expanded from the platform edge toward the platform interior—consistent with the aforementioned vertical and planar facies distribution patterns across ZSQ1 and ZSQ2.

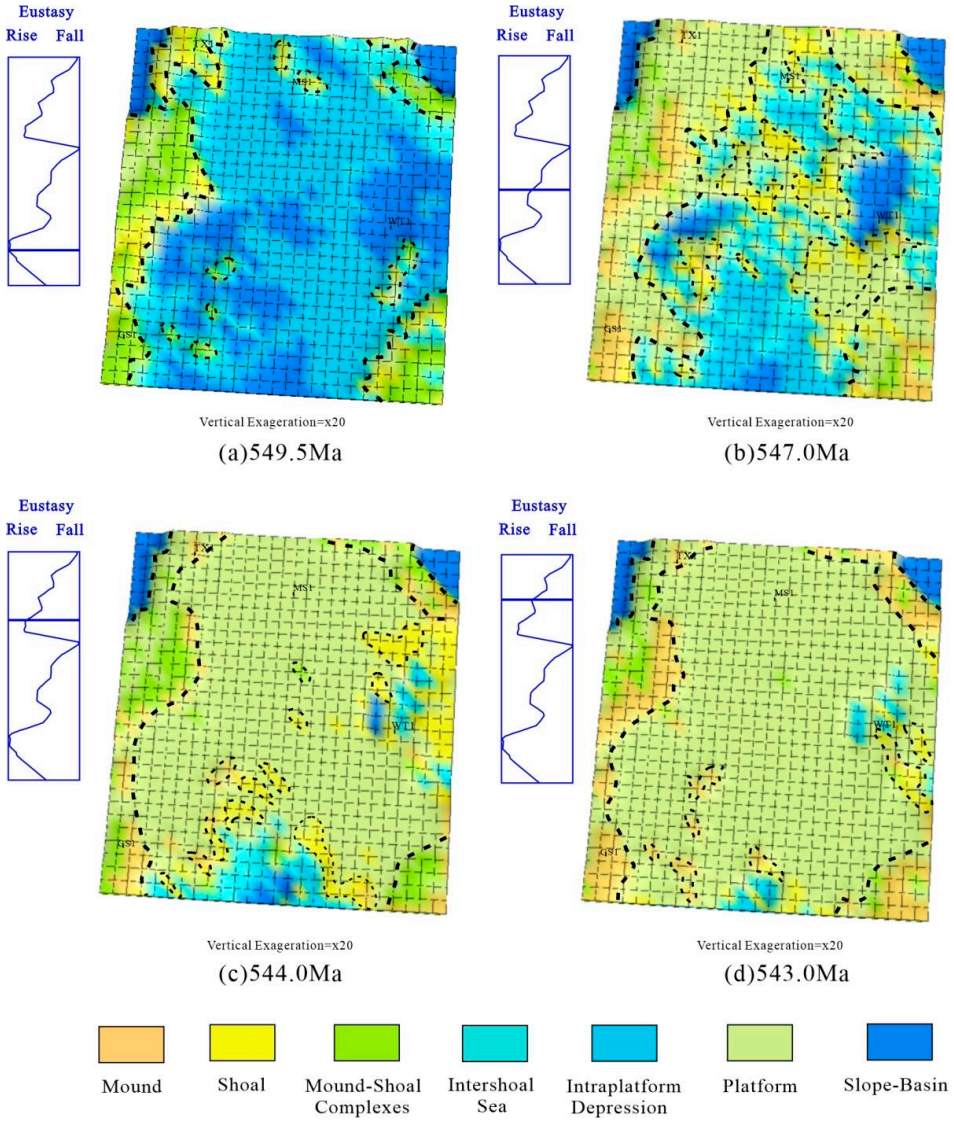


Figure 13. Simulation results of sedimentary facies during different stages of sea level change. (**a**) 549.5 Ma simulated sedimentary facies. (**b**) 547.0 Ma simulated sedimentary facies. (**c**) 544.0 Ma simulated sedimentary facies. (**d**) 543.0 Ma simulated sedimentary facies.

5.3. The Development Position of a High-Energy Facies Belt Reformed by an Ancient Wind Field

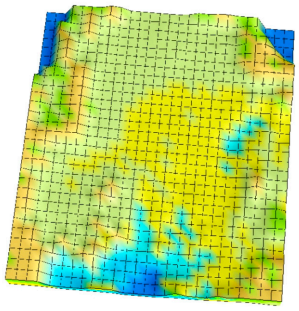
Wind waves control the secondary migration and redistribution of carbonate rocks after deposition. Wind waves affect the spatial distribution of sediments and have a strong transformation effect on sediments. During the Ediacaran period, with the breakup of the Rodinia continent, the Yangtze plate gradually moved to the middle and low latitudes (0–30 °N), mainly affected by the southeast monsoon climate from South Asia and Australia [42,48]. The simulation results are consistent with the Hadley circulation, and the climate is warm and humid at this time.

Under the continuous action of the dominant southeast wind field in the study area, a large-scale continuous distribution of mound–shoal sedimentary system was formed.

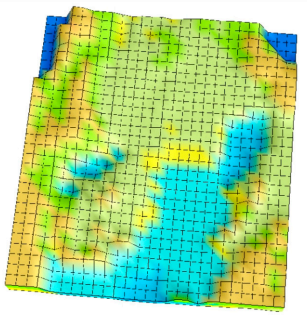
The windward area in the eastern and southern parts of the platform is a high-energy hydrodynamic area. The wave transformation in this area is the most significant. It is the core area for the rapid growth and scale expansion of the reef. It mainly develops high-energy environmental sedimentary subfacies such as mounds and grain shoals. Due to the influence of terrain blocking, the wave energy is obviously attenuated here, and the dynamic strength of the water body is significantly reduced. The sediment is characterized by the alternating sedimentary combination of micritic dolomite and argillaceous dolomite.

Because the study area is controlled by the southeast wind field, through repeated simulation and result feedback, the wave parameters are optimized, and the distribution range of the platform mound–shoal and the platform margin mound–shoal is compared. The wind wave propagation angle is roughly W270° and N15° (Figure 7). By comparing the different results of different parameters, it is found that when the depth of wind and wave action is 10–20 m, the biological (algal) mounds and grain shoals are developed at the depth of the water body, and the carbonate rock yield is high. When the frequency of wave action is 80% and 60%, this is conducive to the development of the mound–shoal complexes. If the frequency is too high, the energy of wave action is too large, which will break the reef-building organisms, forming a wave-resistant skeleton and destroying the formation of mound–shoal complexes (Figure 14).

Number of Waves	Wave A	Wave B
Action Depth (m)	20.0	25.0
Propagation Angle (°)	270	15
Frequency (%)	80	60
Wave Energy (KW/m)	272.8	476.5
Wind Speed (km/h)	61.0	70.4
Wave Period (s)	6.8	7.6
Wave Height (m)	7.2	9.0



Number of Waves	Wave A	Wave B
Action Depth (m)	15.0	25.0
Propagation Angle (°)	270	15
Frequency (%)	100	60
Wave Energy (KW/m)	132.9	376.5
Wind Speed (km/h)	51.4	60.4
Wave Period (s)	5.9	7.6
Wave Height (m)	5.4	8.2



Number of Waves	Wave A	Wave B
Action Depth (m)	20.0	15.0
Propagation Angle (°)	270	15
Frequency (%)	80	60
Wave Energy (KW/m)	272.8	132.9
Wind Speed (km/h)	61.0	51.4
Wave Period (s)	6.8	5.9
Wave Height (m)	7.2	5.4

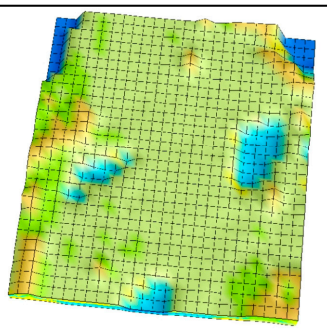


Figure 14. Effects of different grades of wind-generated waves on carbonate sedimentation.

6. Conclusions

(1) The platform margin and restricted platform facies are developed in the northeastern Sichuan Basin, which can be divided into four subfacies: microbial (algal) mound, grain shoal, intershoal sea, and intraplatform depression. Microbial (algal) mound and grain shoal are often superimposed on each other in the form of mound–shoal complexes, which are widely developed at the edge of the platform and sporadically developed in the platform. The intershoal sea and intraplatform depression subfacies are developed in the intraplatform position. The lithology of the two is similar to that of micritic dolomite, but siliceous dolomite can be formed locally in the intraplatform depression and usually the lithology thickness is large.

(2) In this paper, Dionisos software os used to dynamically simulate the lithofacies paleogeographic deposition process of the Ediacaran Dengying Formation in the northeastern Sichuan Basin. The key variables such as accommodation space, carbonate rock yield, and wave energy coefficient are parameterized, and the key influencing factors are identified. The three-dimensional dynamic simulation of the carbonate rock deposition process is performed, and the main controlling factors affecting the distribution of lithofacies paleogeography are discussed.

(3) The distribution of lithofacies paleogeography is controlled by the following three factors: paleogeomorphology determines the type of sedimentary facies and the distribution of lithofacies paleogeography, sea level change controls the superimposed mode and development scale of mound–shoal complexes, and paleowind field affects the redistribution process of sediments. The coupling of these three types of elements jointly shapes the distribution characteristics of the sedimentary system. Among them, the paleogeomorphology provides the sedimentary basement, the lake level fluctuation controls the accommodation space, and the wind wave action transforms the sedimentary distribution and finally forms the paleogeographic pattern of the double-platform margin rimmed platform in the study area.

Author Contributions: Conceptualization, S.L.; methodology, J.L.; software, X.C.; validation, X.C., Y.Z. and D.Z.; investigation, Y.Z. and D.Z.; data curation, X.C.; writing—original draft, X.C.; writing—review and editing, S.L. and J.L.; supervision, D.Z. and S.S.; project administration, D.Z. and S.S.; funding acquisition, S.L. All authors have read and agreed to the published version of the manuscript.

Funding: This research was funded by the National Natural Science Foundation of China (NSFC), under grant number 41902117, under the project titled "Depositional evolution and its response to the paleo-East Asian monsoon climate of lacustrine carbonate rocks in the Middle Eocene of the Dongying Sag".

Data Availability Statement: The original contributions presented in this study are included in the article. Further inquiries can be directed to the corresponding author.

Conflicts of Interest: Author Dazhi Zhang and Shan Sun were employed by the company Exploration and Development Research Institute of PetroChina Daqing Oilfield Co., Ltd. The remaining authors declare that the research was conducted in the absence of any commercial or financial relationships that could be construed as a potential conflict of interest.

References

1. Zou, C.; Du, J.; Xu, C.; Wang, Z.; Zhang, B.; Wei, G.; Wang, T.; Yao, G.; Deng, S.; Liu, J.; et al. Formation, distribution, resource potential, and discovery of Sinian–Cambrian giant gas field, Sichuan Basin, SW China. *Pet. Explor. Dev.* **2014**, *41*, 306–325. [CrossRef]
2. Ma, X.; Yang, Y.; Wen, L.; Luo, B. Distribution and exploration direction of medium- and large-sized marine carbonate gas fields in Sichuan Basin, SW China. *Pet. Explor. Dev.* **2019**, *46*, 1–15. [CrossRef]

3. Wei, G.; Xie, Z.; Yang, Y.; Li, J.; Yang, W.; Zhao, L.; Yang, C.; Zhang, L.; Xie, W.; Jiang, H.; et al. Formation conditions of Sinian–Cambrian large lithologic gas reservoirs in the north slope area of central Sichuan Basin, SW China. *Pet. Explor. Dev.* **2022**, *49*, 963–976. [CrossRef]
4. Li, Z.Q.; Liu, J.; Li, Y.; Hang, W.; Hong, H.; Ying, D.; Chen, X.; Liu, R.; Duan, X.; Peng, J. Formation and evolution of Weiyuan-Anyue extension-erosion groove in Sinian system, Sichuan Basin. *Pet. Explor. Dev.* **2015**, *42*, 26–33. (In Chinese) [CrossRef]
5. Wang, W.Z.; Wen, L.; Yao, J.; Li, K.; He, Y.; Zhou, H.; Nie, J.; Li, Y. Sequence classification and discovery of multi-stage platform margin belts of Sinian Dengying Formation, Sichuan Basin. *Nat. Gas Explor. Dev.* **2019**, *42*, 46–54. (In Chinese)
6. Zhou, H.; Li, W.; Zhang, B.; Liu, J.; Deng, S.; Zhang, S.; Shan, X.; Zhang, J.; Wang, X.; Jiang, H. Formation and evolution of intraplatform basin from the late Sinian to early Cambrian in Sichuan Basin, China. *Pet. Res.* **2017**, *2*, 41–53. [CrossRef]
7. Li, Y.; He, D.; Li, D.; Li, S.; Wo, Y.; Li, C.; Huang, H. Ediacaran (Sinian) palaeogeographic reconstruction of the Upper Yangtze area, China, and its tectonic implications. *Int. Geol. Rev.* **2020**, *62*, 1485–1509. [CrossRef]
8. Zhou, J.; Zhang, J.; Deng, H.; Chen, Y.; Hao, Y.; Li, W.; Gu, M.; Luo, X. Lithofacies paleogeography and sedimentary model of Sinian Dengying Fm in the Sichuan Basin. *Nat. Gas Ind. B* **2017**, *4*, 217–224. [CrossRef]
9. Wang, Z.; Jiang, H.; Chen, Z.; Liu, J.; Ma, K.; Li, W.; Xie, W.; Jiang, Q.; Zhai, X.; Shi, S.; et al. Tectonic paleogeography of Late Sinian and its significances for petroleum exploration in the middle-upper Yangtze region, South China. *Pet. Explor. Dev.* **2020**, *47*, 946–961. [CrossRef]
10. Li, Y.; Wang, X.; Feng, M.; Zeng, D.; Xie, S.; Fan, R.; Wang, L.; Zeng, T.; Yang, X. Reservoir characteristics and genetic differences between the second and fourth members of Sinian Dengying Formation in northern Sichuan Basin and its surrounding areas. *Pet. Explor. Dev.* **2019**, *46*, 54–66. [CrossRef]
11. Harbaugh, J.W. *Mathematical Simulation of Marine Sedimentation with IBM 7090/7094 Computers*; Stanford University: Stanford, CA, USA, 1966; pp. 1–54. [CrossRef]
12. Warrlich, G.; Bosence, D.; Waltham, D.; Wood, C.; Boylan, A.; Badenas, B. 3D stratigraphic forward modelling for analysis and prediction of carbonate platform stratigraphies in exploration and production. *Mar. Pet. Geol.* **2008**, *25*, 35–58. [CrossRef]
13. Berra, F.; Lanfranchi, A.; Smart, P.L.; Whitaker, F.; Ronchi, P. Forward modelling of carbonate platforms: Sedimentological and diagenetic constraints from an application to a flat-topped greenhouse platform (Triassic, Southern Alps, Italy). *Mar. Pet. Geol.* **2016**, *78*, 636–655. [CrossRef]
14. Lanteaume, C.; Fournier, F.; Pellerin, M.; Borgomano, J. Testing geologic assumptions and scenarios in carbonate exploration: Insights from integrated stratigraphic, diagenetic, and seismic forward modeling. *Lead. Edge* **2018**, *37*, 672–680. [CrossRef]
15. Snieder, S.; Griffiths, C.M.; Howell, J.A.; Hartley, A.J.; Owen, A. Quantifying the sensitivity of distributive fluvial systems to changes in sediment supply and lake level using stratigraphic forward modelling. *Sedimentology* **2023**, *70*, 2196–2219. [CrossRef]
16. Zhang, W.; Duan, T.; Liu, Z.; Yuan, S.; Lin, Y.; Xu, H. Application of multi-point geostatistics in deep-water turbidity channel simulation: A case study of Plutonio oilfield in Angola. *Pet. Explor. Dev.* **2016**, *43*, 443–450. [CrossRef]
17. Liu, L.; Li, T.; Ma, C. Research on 3D Geological Modeling Method Based on Deep Neural Networks for Drilling Data. *Appl. Sci.* **2024**, *14*, 423. [CrossRef]
18. Whitaker, F.F.; Felce, G.P.; Benson, G.S.; Amour, F.; Mutti, M.; Smart, P.L. Simulating flow through forward sediment model stratigraphies: Insights into climatic control of reservoir quality in isolated carbonate platforms. *Pet. Geosci.* **2014**, *20*, 27–40. [CrossRef]
19. Resor, P.G.; Flodin, E.A. Forward modeling synsedimentary deformation associated with a prograding steep-sloped carbonate margin. *J. Struct. Geol.* **2010**, *32*, 1187–1200. [CrossRef]
20. De Paula Faria, D.L.; Dos Reis, A.T.; De Souza, O.G., Jr. Three-dimensional stratigraphic-sedimentological forward modeling of an Aptian carbonate reservoir deposited during the sag stage in the Santos basin, Brazil. *Mar. Pet. Geol.* **2017**, *88*, 676–695. [CrossRef]
21. Liu, K.Y.; Liu, J.L. Application of basin modeling method coupling sedimentary filling evolution with petroleum system in simulating ultra-deep oil-gas accumulations: A case study of Sinian Dengying Formation in central Sichuan Basin. *Acta Pet. Sin.* **2023**, *44*, 1445–1458. (In Chinese)
22. Wen, L.; Yang, Y.; You, C.; Zhang, X.; Peng, H.; Wang, W.; Luo, B.; Luo, W. Characteristics of Dengying Fm sedimentary sequence in the central–western Sichuan Basin and their controlling effect on gas accumulation. *Nat. Gas Ind. B* **2017**, *3*, 428–438. [CrossRef]
23. Shang, J.; Feng, M.; Wang, X.; Xia, M.; Li, Y.; Chen, J.; Zhang, C.; Liu, X. Depositional environments of a mixed siliciclastic-carbonate system: A case study of the late Ediacaran sedimentary succession in the northern Sichuan Basin (SW China). *J. Asian Earth Sci.* **2026**, *298*, 106942. [CrossRef]
24. Xie, W.R.; Jiang, H.; Ma, S.Y.; Wang, Z.; Hao, T.; Fu, X.; Su, N.; Li, W.; Wu, S.; Wang, X.; et al. Sedimentary evolution characteristics and favorable exploration directions of Deyang-Anyue Rift within the Sichuan Basin in Late Sinian-Early Cambrian. *Nat. Gas Geosci.* **2022**, *33*, 1240–1250. (In Chinese)
25. Wei, G.; Yang, W.; Du, J.; Xu, C.; Zou, C.; Xie, W.; Zeng, F.; Wu, S. Geological features of Sinian-Early Cambrian intracratonic rift of the Sichuan Basin. *Nat. Gas Ind. B* **2015**, *2*, 37–48. [CrossRef]

26. Ding, Y.; Li, Z.; Liu, S.; Song, J.; Zhou, X.; Sun, W.; Zhang, X.; Li, S.; Ran, B.; Peng, H.; et al. Sequence stratigraphy and tectono-depositional evolution of a late Ediacaran epeiric platform in the upper Yangtze area, South China. *Precambrian Res.* **2021**, *354*, 106077. [CrossRef]
27. Tan, L.; Liu, H.; Chen, K.; Ni, H.; Zhou, G.; Zhang, X.; Yan, W.; Zhong, Y.; Lyu, W.; Tan, X.; et al. Sequence sedimentary evolution and reservoir distribution in the third and fourth members of Sinian Dengying Formation, Gaomo area, Sichuan Basin, SW China. *Pet. Explor. Dev.* **2022**, *49*, 1004–1018. [CrossRef]
28. Chen, Y.; Shen, A.; Pan, L.; Zhang, J.; Wang, X. Features, origin and distribution of microbial dolomite reservoirs: A case study of 4th Member of Sinian Dengying Formation in Sichuan Basin, SW China. *Pet. Explor. Dev.* **2017**, *44*, 745–757. [CrossRef]
29. Wen, H.G.; Wen, L.; Ding, Y.; Zhou, G.; Yan, W.; Ma, K.; Zhong, Y.; Wang, W.; Zhang, Y.; Wu, L.; et al. Rock types and sedimentary facies division scheme of the Sinian Dengying Formation dolomite in the Sichuan Basin and its periphery. *Nat. Gas Ind.* **2024**, *44*, 27–41. (In Chinese)
30. Hoogendoorn, R.M.; Overeem, I.; Storms, J.E.A. Process-response modeling of fluvio-deltaic stratigraphy. *Comput. Geosci.* **2008**, *34*, 1394–1416. [CrossRef]
31. Csato, I.; Granjeon, D.; Catuneanu, O.; Baum, G.R. A three-dimensional stratigraphic model for the Messinian crisis in the Pannonian Basin, eastern Hungary. *Basin Res.* **2013**, *25*, 121–148. [CrossRef]
32. Yin, X.D.; Huang, W.; Wang, P.F.; Wang, J.; Wang, Q.; Yan, D.; Zhou, X. Sedimentary evolution of overlapped sand bodies in terrestrial faulted lacustrine basin: Insights from 3D stratigraphic forward modeling. *Mar. Pet. Geol.* **2017**, *86*, 1431–1443. [CrossRef]
33. Yin, X.D.; Lu, S.F.; Wang, P.F.; Wang, Q.; Wang, W.; Yao, T. A three-dimensional high-resolution reservoir model of the Eocene Shahejie Formation in Bohai Bay Basin, integrating stratigraphic forward modeling and geostatistics. *Mar. Pet. Geol.* **2017**, *82*, 362–370. [CrossRef]
34. Zhang, C.C.; Scholz, C.A.; Harris, A.D. Sedimentary fills and sensitivity analysis of deep lacustrine facies in multi-segment rift basins: Insights from 3D forward modeling. *Sediment. Geol.* **2020**, *408*, 105753. [CrossRef]
35. Condon, D.; Zhu, M.; Bowring, S.; Wang, W.; Yang, A.; Jin, Y. U-Pb ages from the neoproterozoic Doushantuo Formation, China. *Science* **2005**, *308*, 95–98. [CrossRef]
36. Mallarino, G.; Goldstein, R.H.; Stefano, P.D. New approach for quantifying water depth applied to the enigma of drowning of carbonate platforms. *Geology* **2002**, *30*, 783–786. [CrossRef]
37. Porta, G.D.; Kenter, J.A.M.; Bahamonde, J.R. Microfacies and paleoenvironment of *Donezella* accumulations across an upper Carboniferous high-rising carbonate platform (Austurias, NW Spain). *Facies* **2002**, *46*, 149–168. [CrossRef]
38. Lu, G.; He, D.F.; Kai, B.Z. Tectonic subsidence characteristics of Sichuan Basin and its enlightenment to basin genesis. *Chin. J. Geol.* **2023**, *58*, 86–104. (In Chinese)
39. Schlager, W. *Sedimentology and Sequence Stratigraphy of Reefs and Carbonate Platforms*; American Association of Petroleum Geologists: Tulsa, OK, USA, 1992.
40. Gagan, M.K.; Ayliffe, L.K.; Hopley, D.; Cali, J.A.; Mortimer, G.E.; Chappell, J.; McCulloch, M.T.; Head, M.J. Temperature and surface-ocean water balance of the mid-Holocene tropical western Pacific. *Science* **1998**, *279*, 1014–1018. [CrossRef]
41. Sprachta, S.; Camoin, G.; Golubic, S.; Le Campion, T. Microbialites in a modern lagoonal environment: Nature and distribution, Tikehau atoll (French Polynesia). *Palaeogeogr. Palaeoclimatol. Palaeoecol.* **2001**, *175*, 103–124. [CrossRef]
42. Li, Z.X.; Evans, D.A.D.; Halverson, G.P. Neoproterozoic glaciations in a revised global palaeogeography from the breakup of Rodinia to the assembly of Gondwanaland. *Sediment. Geol.* **2013**, *294*, 219–232. [CrossRef]
43. Zhao, G.; Wang, Y.; Huang, B.; Dong, Y.; Li, S.; Zhang, G.; Yu, S. Geological reconstructions of the East Asian blocks: From the breakup of Rodinia to the assembly of Pangea. *Earth-Sci. Rev.* **2018**, *186*, 262–286. [CrossRef]
44. Hu, Y.; He, W.X.; Guo, B.C. Combining sedimentary forward modeling with sequential Gauss simulation for fine prediction of tight sandstone reservoir. *Mar. Pet. Geol.* **2020**, *112*, 104044. [CrossRef]
45. Gu, Z.; Yin, J.; Jiang, H.; Li, Q.; Zhai, X.; Huang, P.; Peng, P.; Yang, F.; Zhang, H. Discovery of Xuanhan-Kaijiang Paleouplift and its significance in the Sichuan Basin, SW China. *Pet. Explor. Dev.* **2016**, *43*, 976–987. [CrossRef]
46. Nie, G.; He, D.; Zhang, Q.; Li, X.; Ji, S.; Mo, G.; Zhang, M. Differential Karst Control of Carbonate Reservoirs: A Case Study of the Fourth Member of Sinian Dengying Formation in Gaoshiti-Moxi, Sichuan Basin, SW China. *Minerals* **2025**, *15*, 1314. [CrossRef]
47. Houck, K.J. Effects of sedimentation, tectonics, and glacio-eustasy on depositional sequences, Pennsylvanian Minturn Formation, north-central Colorado. *AAPG Bull.* **1997**, *81*, 1510–1533. [CrossRef]
48. Narbonne, G.M.; Xiao, S.; Shields, G.A.; Gehling, J.A. The Ediacaran Period. In *The Geologic Time Scale*; Elsevier: Oxford, UK, 2012; Volume 1, pp. 413–435. [CrossRef]

Disclaimer/Publisher's Note: The statements, opinions and data contained in all publications are solely those of the individual author(s) and contributor(s) and not of MDPI and/or the editor(s). MDPI and/or the editor(s) disclaim responsibility for any injury to people or property resulting from any ideas, methods, instructions or products referred to in the content.